Jurnal Kejuruteraan 34(6) 2022: 1237-1250
https://doi.org/10.17576/jkukm-2022-34(6)-24

Enhancement of Aerodynamic Performance of High Speed Train Through Nose Profile Design: A Computational Fluid Dynamics Approach

Khurram Hameed Mughal*, Salman Abubakar Bugvi, Muhammad Fawad Jamil, Basim Tamoor Baig, Taha Ahmad, Muhammad Irfan Ashraf, Abdul Ahad & Ali Abdullah Gondal

Mechanical Engineering Department, The University of Lahore, Lahore, Punjab, Pakistan

**Corresponding author: khurram.hameed@me.uol.edu.pk*

Received 22 February 2022, Received in revised form 27 May 2022
Accepted 27 June 2022, Available online 30 November 2022

ABSTRACT

Aerodynamic drag of fast-moving train has significant impact on its fuel consumption and design safety. To improve aerodynamic performance, the drag forces on the train surfaces must be reduced. Train's front-end nose design has boundless geometrical variations that can be applied for improved performance. Three geometric characteristics were used in present research: A-pillar roundness, nose length that controls its shrinking, and nose bluntness. Latin-Hypercube based random sampling method was used to determine appropriate values of these parameters for specific range. Using Computational Fluid Dynamics (CFD), a numerical approach was used to analyze train aerodynamic performance based on selected factors and operating conditions. Comparisons based on analysis of the base design and proposed design models were made and evaluated for enhanced performance. CFD analysis of the base design and iterative improvements in modified designs indicate drag reduction through change in A-pillar roundness and bluntness of nose to be 10% and 22%, respectively. The increase in nose length which controls nose shrinkage causes the drag to increase by 35%. Similarly, the boundary layer and pressure distribution on the front end of train were also considered and analyzed for performance improvement. It was concluded that the length controlling nose shrinkage of proposed train design is the key factor among the selected geometric parameters that has more influence on drag on high-speed train surface in comparison to other parameters considered. This research effort offers a modification, analysis and comparison of front-end nose geometry of high-speed train to improve aerodynamic performance and consequently fuel consumption.

Keywords: Computational Fluid Dynamics (CFD); boundary layer; train nose profile; pressure distribution; high-speed train; aerodynamic drag

INTRODUCTION

The China Pakistan Economic Corridor (CPEC) is being developed for the Logistics Supply Chain Development of the region with connectivity, communication and infrastructure. The Main Line 1 railway track is planned to be developed in phases during the next 5 years. This initiative will bring high speed passenger and freight trains to Pakistan requiring initiation, planning, execution and Controlling (Bugvi et al. 2021). These trains increase mobility, connectivity, provide logistics and reduce travel time. The design and development of such trains with enhanced performance is an ongoing engineering activity being undertaken at advanced countries' industries and institutes (Zhou & Shen 2019). As a complex and advanced engineering transport solution, high speed train involves mechanical, electrical, communication and control mechanisms. A number of factors such as acoustics, aerodynamics, structural, dynamic and fatigue characteristics are involved in design of the high-speed train (Zhang, 2014). The operational problems faced by the high-speed train pertaining to corrugation, vibration, misalignment and noise have been highlighted in previous studies (Jin 2018). The design variables can be handled for optimization which is an ongoing process to make lighter and faster high-performance trains.

The advancement and progress in the design of high-speed trains started in Japan in 1964. European and other advanced countries also adopted the evolution in high-speed railway technologies. The first-generation technology pertained to speeds up to 200 kph followed by second generation till 300 kph. The current generation is the third one with ambition to approach speeds more than 350 kph (Chen et al. 2017). The challenge to push the speed limit and achieve 3G railway technology involves massive design improvements. All high-speed trains are designed to meet service reliability and safety standards. Safety standards involves protection against derailment or stoppages and safe passage of the train. Service reliability is related to factors such as fatigue, noise, vibration and speed. The other factors including the design of rail track, the pantograph, catenary arrangement, train aerodynamics and design also contribute towards the complexity of transport system. Various fields of

Mechanical, electrical, communication, electronics, Safety and Management combine together to enable creation of an advanced high speed railway technology system (Viviani et al. 2021).

One of the key factors in reducing the energy consumption, sound and vibration of the high-speed train is its aerodynamic as well as structural design. The nose design of the train is of special interest and has been focused upon by various researchers (Li et al. 2019; Munoz et al. 2015; Munoz-Paniagua et al. 2014 and Niu et al. 2018). During the travel at high speed, the drag and lift forces impact the key performance factors (Muñoz-Paniagua et al. 2020). The analysis of the slipstreams in high-speed trains is also an area to explore (Zampieri et al. 2020). The wake region created at the end of the tail car also causes reduction in speed and train performance (Raghunathan et al. 2002). The design of the train nose, length of the train, crosswinds (Muñoz-Paniagua and Garcia, 2019; Niu et al. 2017) open channel (Miyachi et al. 2020), tunnel passage (Li et al. 2017), and platforms (Niu et al. 2020) all have an impact on the train performance. The aerodynamic properties of the surrounding air are incompressible and highly turbulent at the train speed attained.

Various studies have been carried out to explore the combination of design models created by varying design parameters through numerical computations (Muñoz-Paniagua and Garicia 2020). Computational Fluid Dynamics is a technique used for analyzing the aerodynamic flow characteristics of the high-speed train under various conditions (Anderson, 1995). Various design models of the existing high-speed train are established and investigated. The design of experiments is used to generate models which are evaluated through CFD analysis for attaining better performance (Viviani et al. 2021). The calculation of Reynold number, an indicator of turbulent flow, is a key parameter in identifying appropriate CFD analysis technique (Niu et al. 2018). The design process has been further extended by researchers to cover optimization methods (Shuanbao et al. 2014). Various design optimization techniques have been implemented to high-speed train for best performance (Li et al. 2019; Munoz et al. 2015).

Various research studies are being undertaken to improve the nose design of the train through variation in profile parameters (Chen et al. 2019). The use of composite material in the nose cone improves strength to weight ratio and reduces the failure rate. The linkage between wheel and track of the train can be investigated and improved through study of contact mechanics, adhesion, fatigue, wear and creep theory. The structural and aerodynamic design of the high-speed train is of importance. The train design encounters various aerodynamic conditions arising from passage through tunnels, open channels, crossover between trains, across platforms and in crosswinds. These varying aerodynamic situations have been investigated in previous works to contribute towards improvement in high-speed train performance. The automation and control system of the 3G trains are improving with enhanced electronics and information technology mechanisms.

The integrated areas of engineering and technology are synthesized to create a safe, reliable and energy efficient transport system for the benefit of the population (Chen et al. 2019). There is a strong relationship between introduction of high-speed railway system to higher usage and profits. Hence continued efforts are needed to improve the design in the individual sections of such high-speed trains. The need is to integrate the technologies in a cohesive manner for greater speeds and performance (Muñoz-Paniagua and Garcia, 2020).

The scope of this study includes the numerical analysis of a high-speed train nose design by varying dimensions of profile to reduce boundary layer thickness and drag. Aerodynamics is one of the major considerations during the design and operation of the high-speed railway system as well as cars and aircrafts (Li et al. 2020). The aerodynamic drag depends on the nose shape, surface contact of the train body with the surrounding air, design of cars, pantograph-roof connection arrangement, train speed and fluid properties. The pressure drags and the wake region at the tail end are also created which influence the performance of high-speed train (Meng et al. 2021). The complexity of design requirements associated with performance improvement is enabled by analysis through Computational Fluid Dynamics. An improvement in design or related mechanisms which can contribute to reducing aerodynamic drag will help achieve high speeds, performance and service reliability (Munoz et al. 2015). The elementary model is based on an actual high-speed train operating in developed country. The model with reduced drag force on the train, pressure gradient and boundary layer thickness, minimizing the wake region behind the tail car, thereby enhancing the fuel economy is selected after numerical computations.

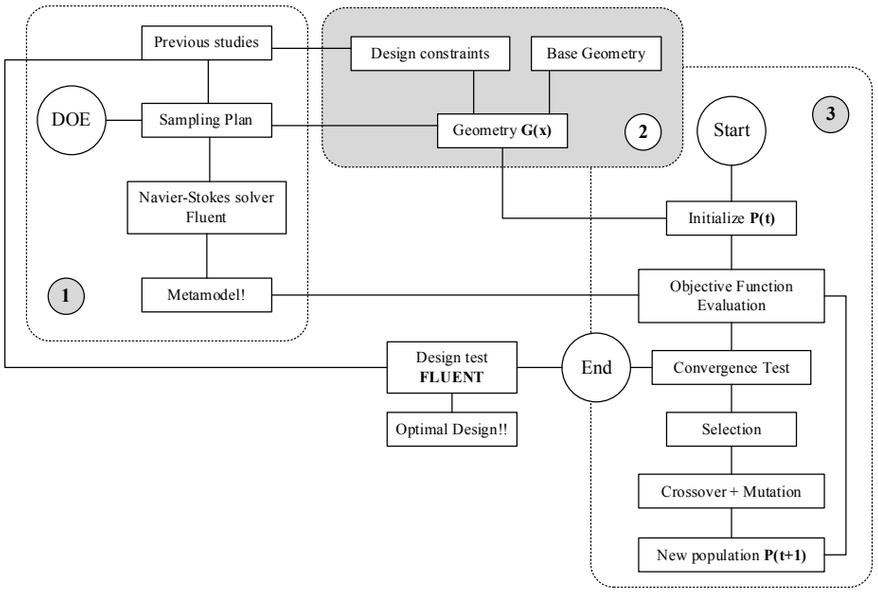

FIGURE 1. Schematic for research methodology and optimization procedure

METHODOLOGY

Numerical model of the front end / nose of the train for aerodynamic analysis was developed using Solid Works software. The CAD model of the train was formed from the initial geometry of a Chinese model train. The design of the front end of the train was modified by incorporating and changing the nose profile dimensions and then analyzing through Computation Fluid Dynamics.

In Figure 1, the flowchart of the sampling plan, the design synthesis and the multi-objective optimization strategy is presented. The process cycle has been divided into three major parts. The first stage includes the sampling strategy and the design of experiments that were used for optimization. In accordance with previous research studies, a sampling plan was constructed. The sampling plan has been solved using the Navier-Stokes equation. The second stage is the model synthesis for various nose geometries. The third stage involves the solution and post processing of the model being synthesized. The solution was performed using a CFD software to calculate the required objective functions. A convergence test was also performed to obtain the solution. Mesh / Grid independence analysis was performed to get reasonably precise numerical results (Mughal et al. 2021, Mughal et al. 2021, Niu et al. 2018).

In this investigation, train nose profile was analyzed by varying nose length (l_1) which controls the shrinking of the nose, parameter (l_2) that controls the bluntness of the nose, and A-pillar roundness (R_1) which is related to the bluntness of the nose tip (Figure 3). In Figure 2, the relationship between design principles, performance indexes and design variable are presented for the aerodynamic analysis of a train body subjected to air drag.

NUMERICAL MODELLING

The numerical modelling of the train front end model is improved from the initial model with geometrical parameters as presented in Table 1. The base model of the train was imported in ANSYS Fluent for the purpose of performing CFD analysis (Paniagua et al. 2014).

In order to optimize a model, techniques such as Genetic algorithms and metamodel definitions can be used to make the number of iterations finite. One such technique "Metamodel" was analyzed in this study which is defined by the linear combination given as follows:

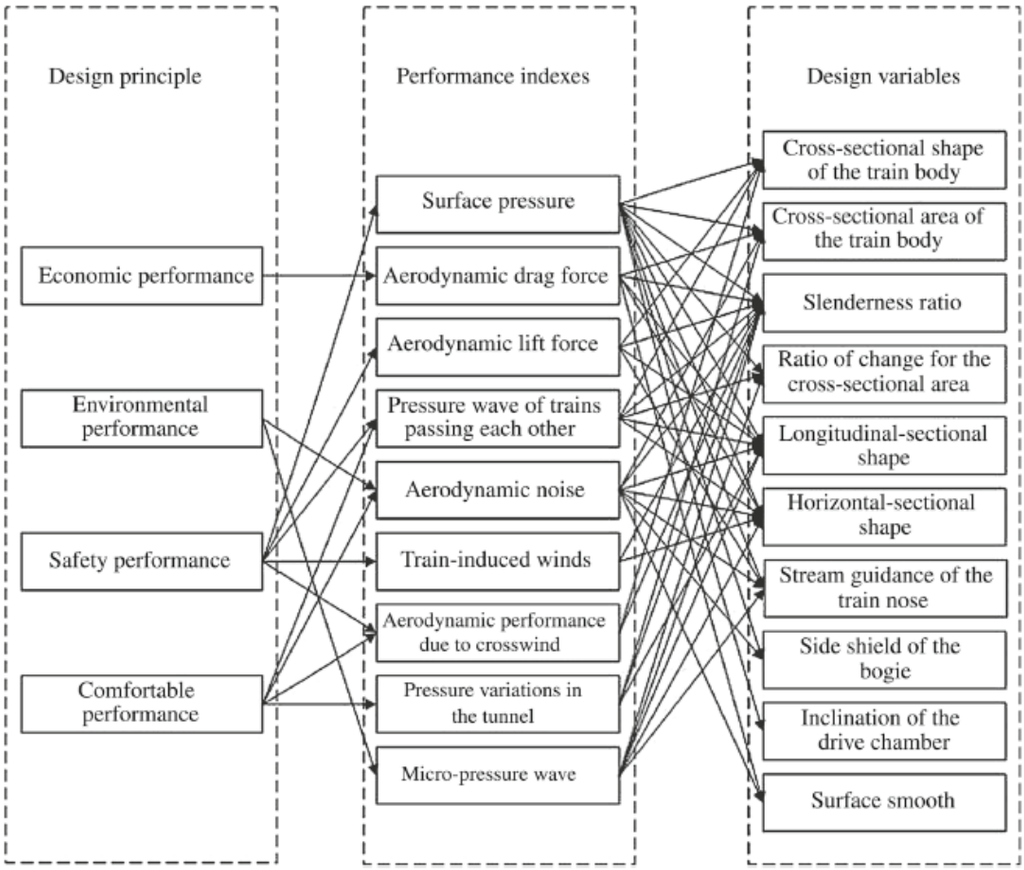

FIGURE 2. Relationship of design principle, performance indexes and design variables of high-speed train (Ding et al. 2016)

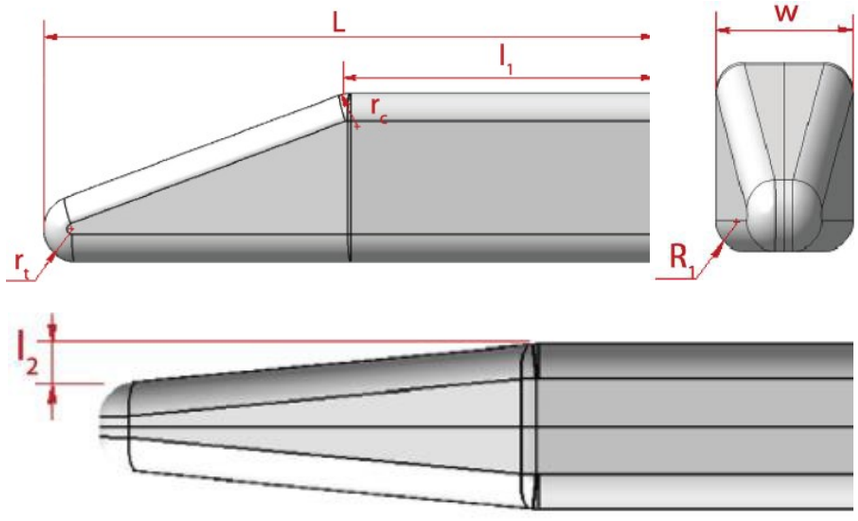

FIGURE 3. Train nose design with geometric parameters for optimization

TABLE 1. Initial geometric parameters of train model

Parameters	Values
Length of train head	15 *m*
Train height	3.85 *m*
Train width	3.00 *m*
Nose length, l_1	3 *m*
Nose bluntness, l_2	1 *m*
A-pillar roundness, R_1	0.75 *m*
Nose tip roundness, r_t	0.75 *m*
Clearance from Ground	0.25 *m*
Radius that controls connections between nose and rest of the car (r_c)	0.75 *m*

$$\hat{y}(\boldsymbol{x}) = \sum_{i=1}^{m} \omega_i \emptyset(|\boldsymbol{x} - \boldsymbol{x_i}|) \tag{1}$$

This approximation contains $\hat{y}(\boldsymbol{x})$ as the estimate of the response. $\emptyset(|\boldsymbol{x} - \boldsymbol{x_i}|)$ represent the radial basis function. Radial function is determined by using following relation (Paniagua et al. 2014).

$$\emptyset(d_i) = \exp\left(-\frac{d_i^2}{2(|\boldsymbol{r_i}|^2)}\right) = \exp\left(-\frac{|\boldsymbol{x} - \boldsymbol{x_i}|^2}{2(|\boldsymbol{r_i}|^2)}\right) \tag{2}$$

A sampling plan was constructed from the initial model to develop design of experiments (DOE) by varying various geometric parameters. The range and sample size were selected based on Latin-Hypercube random sampling method. The Latin-Hypercube method provides a dimensional distribution of the parameter within specified range. The DOE results are given in Table 3.

Compressible and turbulent flow conditions were considered with the speed of the train fixed at 250 *km*/*h*. ANSYS Fluent software was utilized with the standard k-epsilon $(k-\epsilon)$ turbulence model with a second order upwind momentum and time discretization scheme. The $k-\epsilon$ turbulence model is used to simulate the flow characteristics which are dependent on the boundary conditions and the nature of the flow. It is characterized by the transported variable which is the turbulent kinetic energy as well as rate of dissipation of kinetic energy.

The k-epsilon $(k-\epsilon)$ has been used in various relevant research works for the determination of mean flow characteristics through CFD analysis (Muñoz-Paniagua and Garcia, 2014). As the k-epsilon model belongs to Reynold-averaged Navier Stokes (RANS) technique, the turbulent flow characteristics can be analyzed appropriately with reasonable accuracy.

The governing equations for the flow characteristics under consideration are as follows:

For turbulent (k)

$$\frac{\partial(\rho k)}{\partial t} + \frac{\partial(\rho k u_i)}{\partial x_i} = \frac{\partial}{\partial x_j}\left[\frac{\mu_t}{\sigma_k}\frac{\partial(k)}{\partial x_j}\right] + 2\mu_t E_{ij}E_{ij} - \rho\epsilon \tag{3}$$

For dissipation (ϵ)

$$\frac{\partial(\rho\epsilon)}{\partial t} + \frac{\partial(\rho\epsilon u_i)}{\partial x_i} = \frac{\partial}{\partial x_j}\left[\frac{\mu_t}{\sigma_\epsilon}\frac{\partial(\epsilon)}{\partial x_j}\right] + C_{1\epsilon}\frac{\epsilon}{k}2\mu_t E_{ij}E_{ij} - C_{2\epsilon}\rho\frac{\epsilon^2}{k} \tag{4}$$

Here, ρ is the density, t is the time, k is the kinetic turbulent energy, $C_{1\epsilon}$ & $C_{2\epsilon}$ are adjustable constants, ϵ is the dissipation energy and E_{ij} is the energy in the *xy* plane.

The solid body was imported to ANSYS Fluent for the purpose of meshing. Different parts of fluid domain were generated including inlet, outlet, walls, track, nose, train body and tail. Firstly, surface mesh was created using Robust (Octree) method and volume mesh was created using Quick (Delaunay) method. For better mesh quality to achieve reasonably accurate results regarding flow characteristics and capturing the boundary layers, tetragonal mesh was generated as shown in Figure 4 (Paniagua et al. 2014). Total of 6 layers were created around the body. Then, the meshed model was imported to Fluent ANSYS.

The purpose of creating sampling data was to calculate the drag values at different frontal curve radii so that minimum drag values could be identified and calculated. Post processing of CFD model was carried out to investigate the variation of different flow parameters with nose geometry.

TABLE 2. Boundary conditions for CFD analysis of train

Boundary	Boundary Condition	Values
Inlet	Constant Velocity, Turbulent Intensity = 5%, Turbulent Intensity ratio = 10%	v = =69.94 *m/s*
Outlet	Pressure Outlet	Zero Gauge Pressure
Track	Stationary wall Specified Shear	Shear Stress = 0
Train body	No slip- stationary wall	-
Domain Walls (Top and side)	Stationary wall Specified Shear	Shear Stress = 0

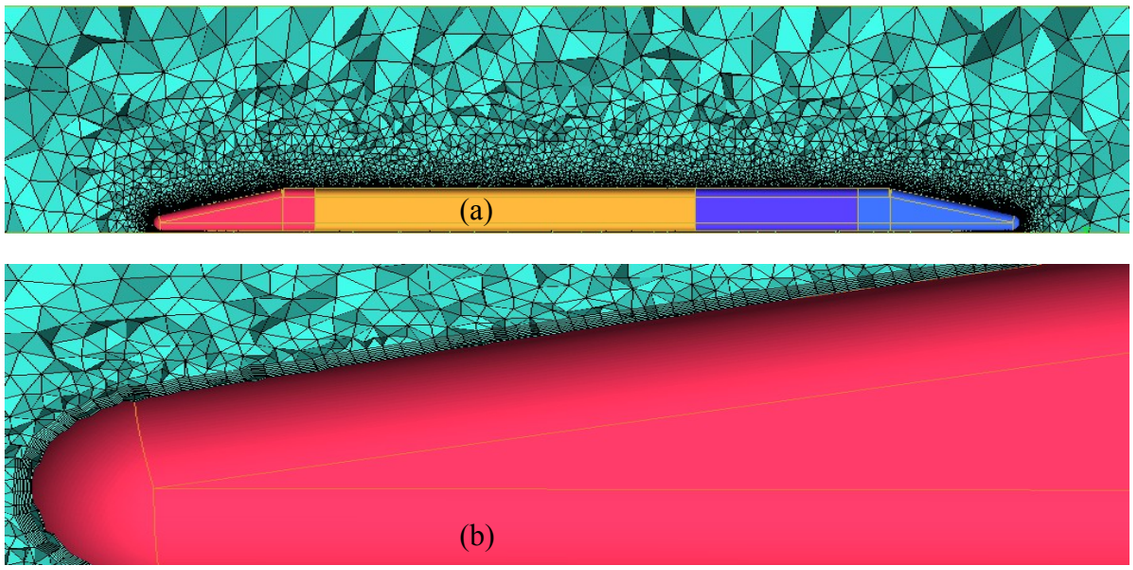

FIGURE 4. Tetrahedral Mesh of Fluid Domain, (b) Prism layers around the train body

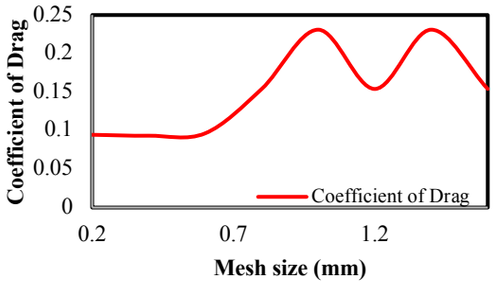

FIGURE 5. Mesh independence analysis

Grid independence analysis was conducted by varying distance of closest point to train surface, mesh resolution in streamwise direction and time step. (Paniagua et al. 2014). Mesh size of fluid domain was varied from coarse near the domain boundary to fine near the train surface. This refinement in the mesh size resulted in the percentage error of less than 2% as presented in Figure 5. Hence, the appropriate mesh size was selected to get reasonably accurate results (Mughal et al. 2021a, Mughal et al. 2021b,, Niu. et al. 2018, Mughal et al. 2022).

RESULTS AND DISCUSSIONS

Model 1 is the cone shaped train design with geometrical parameters l_1 = 6 m, l_2 = 1 m and R_1 = 0.75 m for its performance evaluation using CFD. Contour plot of Figure 6a, shows regions subjected to high pressure under specified flow conditions. Contour plot shows that the maximum pressure occurs at nose. Drag coefficient for model 1 was determined to be 0.0945 and the coefficient of lift was -0.0687. The pressure distribution is dependent on the geometric parameters. The joint between the nose and the back body of the train has medium pressure, while the rest of the train surface has nearly uniform pressure distribution.

Model 2 contains a steeper surface of the front-end nose with the geometrical parameters of l_1 = 9 m, l_2 = 1 m and R_1 = 0.75 m. The numerical simulation on this model shows a maximum pressure distribution on a larger surface area of the nose as compared to model 1, as shown in Figure 6b. The coefficient of drag for this model was calculated to be 0.1053 which is significantly higher than that of model 1. The percentage rise in the coefficient of drag of model 2 with respect to model 1 is 11.4%. The coefficient of lift for model 2 was determined to be -0.1053.

Model 3 has the geometrical parameters equal to l_1 = 12 m, l_2 = 1 m and R_1 = 0.75 m with different nose slope. The pressure contour plot shows the maximum pressure on nose circular end, as indicated in Figure 6c. The coefficient of drag and coefficient of lift for this model were 0.1164 and 0.1261 respectively. The coefficient of drag in Model 3 was observed to be higher than that in Models 1 and 2 due to increase in length which reduces slenderness ratio due to shortened nose shape longitudinal dimension at constant train width causing high pressure gradient. These results were found in good agreement with the findings of Paniagua et al. 2014 and Meng et al. 2021.

Model 4 has the geometrical parameters as l_1 = 3 m, l_2 = 0.5 m and R_1 = 0.75 m with pressure contour plot as shown in Figure 6d. The maximum pressure is exerted on nose circular end. The area under pressure is small in comparison to model 2 and model 3. The coefficient of drag and coefficient of lift for this model are 0.1019 and -0.0833, respectively. The overall percentage decrease in coefficient of drag of model 4 in comparison to model 3 is 12.4%.

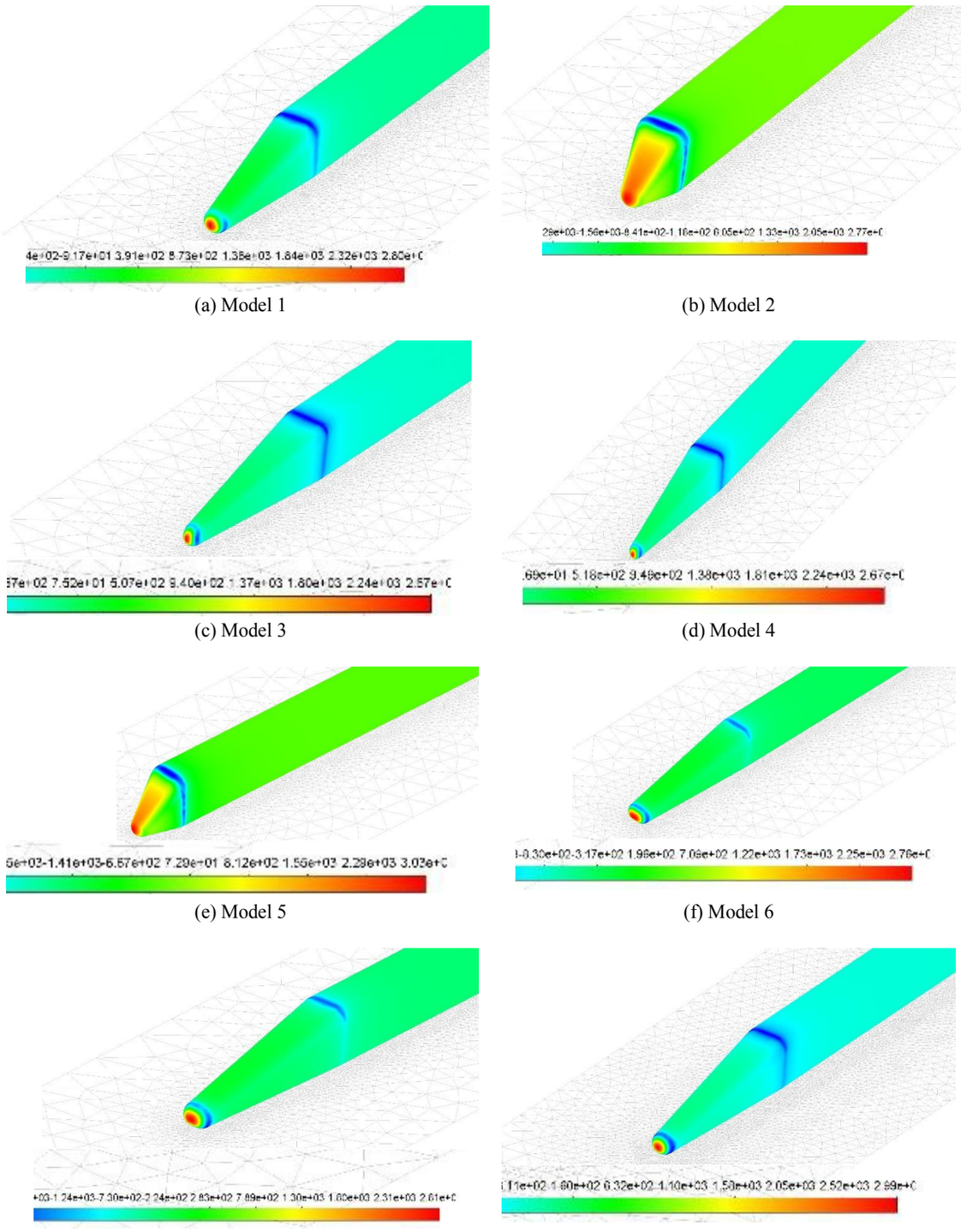

(a) Model 1 (b) Model 2

(c) Model 3 (d) Model 4

(e) Model 5 (f) Model 6

(g) Model 7 (h) Model 8

FIGURE 6. Pressure distribution at nose surface of train models

The model 5 has the geometrical parameters as l_1 = 3 *m*, l_2 = 0.6 *m* and R_1 = 0.75 *m*. The area over which the pressure is distributed is larger in comparison to models 3 and 4, as shown in Figure 6e. The coefficient of drag for this model is 0.0993, while coefficient of lift is -0.0802. The overall percentage decrease in coefficient of drag of model 5 in comparison to model 4 is 2.5%.

With geometrical parameters as l_1 = 3 *m*, l_2 = 0.75 *m* and R_1 = 0.75 *m*, model 6 has smaller area over which the pressure is distributed in comparison to models 4 and 5 as shown in Figure 6f. The coefficient of drag for this model is 0.0986, while coefficient of lift is -0.0643. The overall percentage decrease in coefficient of drag of model 6 in comparison to model 5 is 0.7%. The decrease in coefficient of drag in Model 6 as compared to that of other models is attributed to reduction in pressure gradient with the increase of nose bluntness. Increasing nose bluntness causes the nose sharpness to enhance while reducing the nose cross sectional area that results in pressure gradient and drag coefficient to decrease. Influence of nose bluntness on pressure gradient and drag coefficient are in good agreement with the findings of Ku et al. 2010 and Paniagua et al. 2014.

Model 7 has geometrical parameters as l_1 = 3 *m*, l_2 = 1 *m* and R_1 = 0.5 *m* the area over which the pressure is distributed is nearly similar in comparison to models 5 and 6, as shown in Figure 6g. The coefficient of drag for this model is 0.0934 with coefficient of lift equal to -0.0950. The overall percentage decrease in coefficient of drag of model 7 in comparison to model 6 is 5.2%.

With geometrical parameters as l_1 = 3 *m*, l_2 = 1 *m* and R_1 = 0.6 *m*, model 8 has smaller area over which the pressure is distributed in comparison to models 5, 6 and 7 as shown in Figure 6h. The coefficient of drag for this model is 0.0898. The overall percentage decrease in coefficient of drag of model 8 in comparison with model 7 is 3.8%. The lowest magnitude of drag coefficient in Model 8 is attributed to lowest pressure gradient due to short nose length l_1 and large A-pillar roundness that cause smooth air flow over the train.

The pressure distribution on the train nose geometry indicates the maximum concentration of the pressure at the center of the nose profile. The pressure distribution is larger in models 2 and 5 as compared to other geometric models. These models are the least suitable models due to higher pressure and drag. Reason is attributed to steeper front surfaces in model 2 and model 5 causing maximum pressure of 2.97 *kPa* and 3.02 *kPa* in those models respectively, as compared to other models.

The velocity distribution in train models were also analyzed to identify the regions of maximum / minimum magnitudes and flow pattern. The purpose is to identify the variation of velocity and flow characteristics with various train nose geometric parameters. Referring to Figure 7a, the velocity at the surface is zero primarily due to no-slip condition. Furthermore, the velocity is minimum at the front-end curvature, while maximum at the upper end of nose.

In models 2 and 5, the maximum velocity was observed at the top end of nose, which indicates a localized increase in velocity at that region as compared to other models. The magnitude of the velocity at the front end is also minimum just like model 1. The fluid domain with minimum velocity is mainly due to the aerodynamic drag and boundary layer thickness causing fuel economy to decrease (Figure 7b).

For model 3, the maximum velocity variation is observed at front end of nose with low velocity in remaining fluid domain. The velocity above the train nose was observed to be constant due to the gradual increase in slope of nose profile rather than abrupt variation as in case of base model (Figure 7c).

The model 4 shows similar behavior in terms of velocity profile to model 3, the minimum velocity region is at the curvature while the velocity above the nose profile slope is nearly same. One major difference between model 3 and model 4 is that the region of low velocity in front of the curvature in model 3 is greater in comparison to the other (Figure 7d). Therefore, it can be concluded that the curvature directly effects the low velocity region in front of the nose profile.

Geometry of model 5 is drastically different as compared to models 3 & 4. Velocity contour of the fluid domain demonstrates maximum velocity on the top edge as shown in Figure 7e. Whereas, the velocity near the front-end nose curvature is nearly equal to 0. Hence, this profile has greater drag and consequently fuel consumption.

In model 6, the velocity profile is similar to that of models 3 and 4 (Figure 7f). The front-end nose curvature has minimum velocity with zero velocity at the surface due to no-slip condition.

The velocity profiles of model 6 and 7 are similar in nature. One major difference is the effect of radii which causes the region of low velocity concentration to move near the curvature (Figure 7g). No slip condition at the surface was also observed to exist. The model 8 produces minimum drag with minimum variation in the velocity as indicated by the contour of Figure 7h.

The pressure and velocity contours of the train models provide the elementary data and insight to achieve the optimum train performance in terms of low pressure, high velocity and minimum aerodynamic drag in terms of selected geometric parameters of nose profile. A system study of these selected parameters provides a finite number of computational datasets. These data sets can be used to simulate the specific conditions to obtain optimum performance parameters at low cost and good accuracy through CFD analysis.

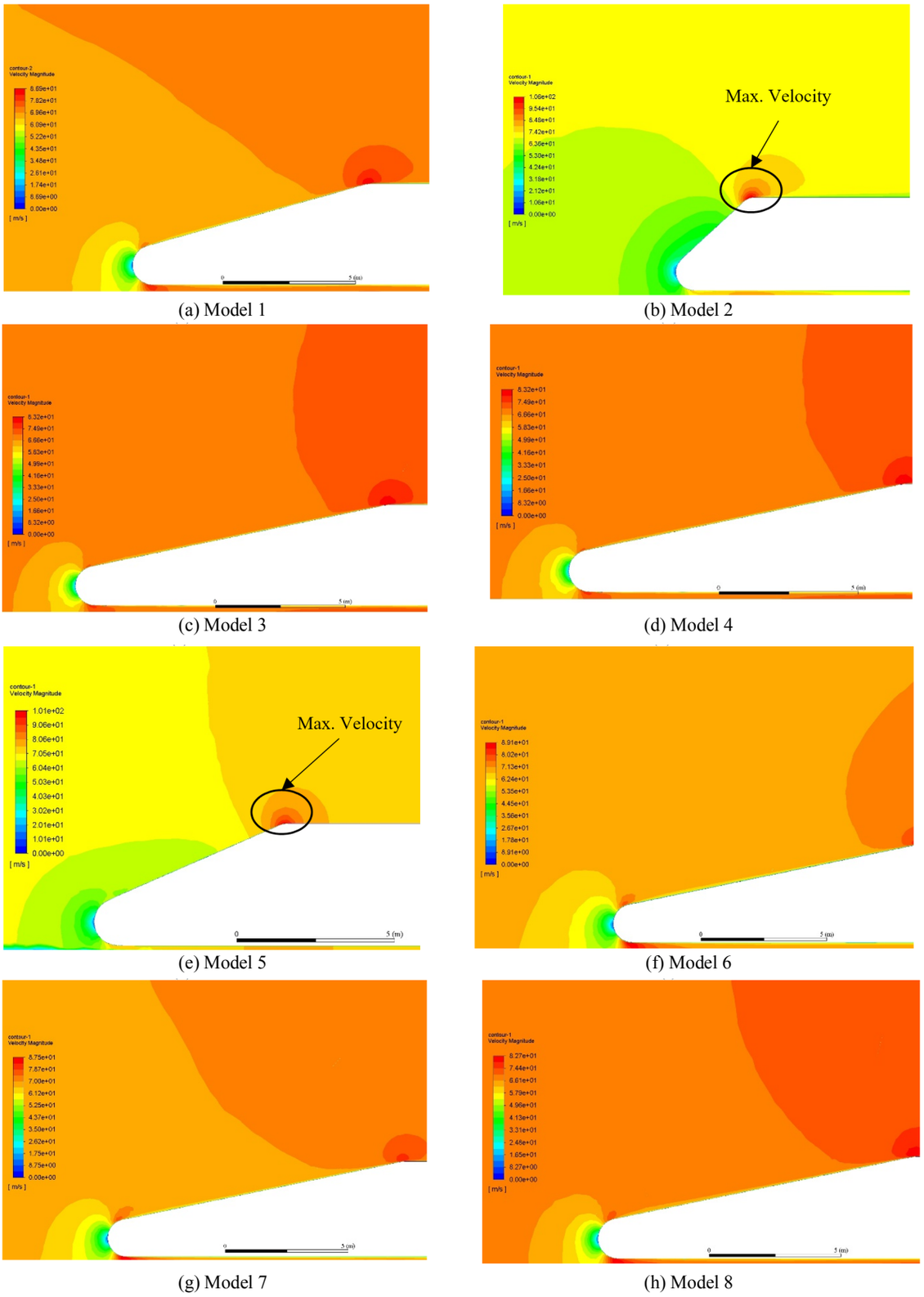

(a) Model 1 (b) Model 2

(c) Model 3 (d) Model 4

(e) Model 5 (f) Model 6

(g) Model 7 (h) Model 8

FIGURE 7. Velocity distribution over the train models

The methodology of the present research was validated with the work of other researchers by considering their models and operating conditions (Paniagua et al. 2014; Meng et al. 2021).

A comparative analysis of the selected models was conducted and the results of the lift and drag coefficients for train nose profiles are presented in Table 3. For this purpose, a three dimensional models of the selected train designs were considered and analyzed using CFD. The Base Model represents the simplified geometry of the train on which the CFD analysis was performed. The base model was initially tested for the determination of performance characteristics under specified conditions (Paniagua et al. 2014). The influence of various geometric parameters of train nose profile on flow characteristics were analyzed for comparison with the base model.

TABLE 3. Lift and drag coefficients for selected Models

Models	l_1 (m)	l_2 (m)	R_1 (m)	Lift	Drag
Model 1	6	1	0.75	-0.0687	0.0945
Model 2	9	1	0.75	-0.1338	0.1053
Model 3	12	1	0.75	-0.1261	0.1164
Model 4	3	0.5	0.75	-0.0833	0.1019
Model 5	3	0.6	0.75	-0.0802	0.0993
Model 6	3	0.75	0.75	-0.0643	0.0986
Model 7	3	1	0.5	-0.0950	0.0934
Model 8	3	1	0.6	-0.097	0.0898

A-pillar roundness (R_1) has been varied between $0.5m$ and $0.75m$ for determination of coefficient of drag (C_D). Pressure distribution and variation over the train surface were observed to have an association with drag force. Numerical simulation results show that the coefficient of drag decreases from 0.094 at minimum nose roundness to 0.084 at maximum roundness indicating a linearly decreasing trend (Figure 8a). A decrease in drag of about 11.7% was observed with the variation of roundness R_1. The decrease of drag is attributed to the smooth air flow over the improved train nose profile by increasing A-pillar roundness.

The effect of bluntness of the nose (l_2) on the coefficient of drag shows a linearly decreasing trend (Figure 8b). The bluntness is varied between $3m$ to $11m$ to obtain the drag value through numerical simulation. The range of the variation of the coefficient of drag was between 0.11 and 0.085. The overall percentage decrease in the drag coefficient (C_D) with the increase of nose bluntness (l_2) was about 22.7% indicating a strong decreasing relationship between nose bluntness and drag. The decrease of drag coefficient with the increase of nose bluntness is attributed to the increase of sharpness and reduction of cross sectional area by enhancing nose bluntness. Paniagua et al. (2014) also found the coefficient of drag to decrease with the increase of nose bluntness, therefore, the present results are in accordance with the work of other researchers. However, their study was slightly different and focused on CFD analysis of train entering a tunnel.

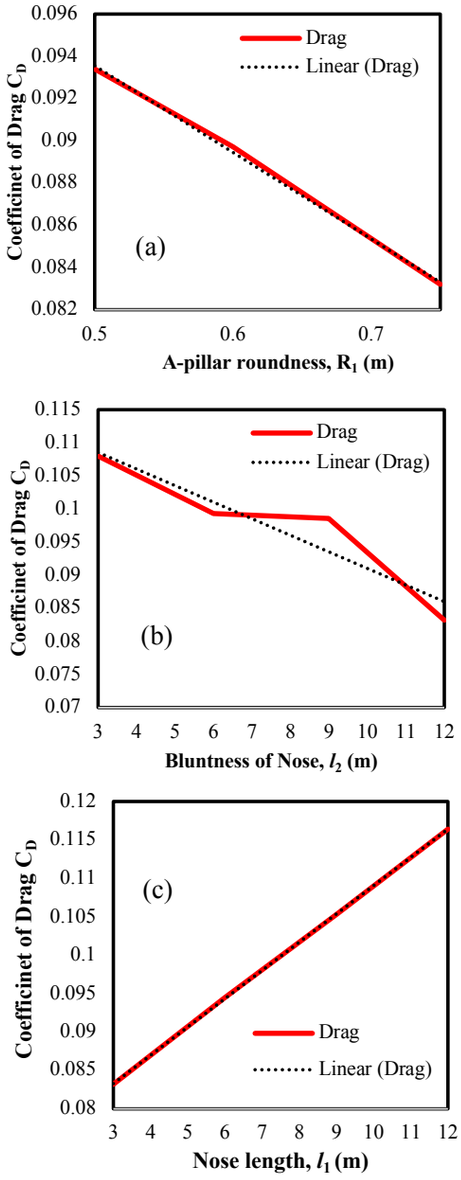

FIGURE 8. Variation of drag coefficient with (a) A-pillar roundness, (b) nose bluntness and (c) nose length

Similarly, the relationship between nose length (l_1) and the coefficient of drag was obtained through simulation for wider range of l_1 between $3m$ and $11m$. Based on the numerical results, it is observed that the increase in the nose length (l_1) causes the coefficient of drag to increase (Figure 8c). This occurred due to increase of pressure gradient with the nose length (l_1). Furthermore, increase of parameter l_1 forces the nose shape longitudinal dimension to decrease, ultimately reducing the slenderness ratio due to constant train width. This causes generation of stronger recirculation region which enhances the effective blockage ratio. Paniagua et al. (2014) found the coefficient of drag to

increase with the increase of pressure gradient, therefore, the present results are in accordance with the work of other researchers. For selected range of nose length, drag on the train surface varies between 0.084 till 0.115 indicating an increase of about 37%. By comparing the effects of the three factors (R_1, l_2 & l_1) based on the percentage decrease in drag, the nose length is the most influential parameter resulting in variation of drag considering the specified operating condition.

Figure 9a shows the pressure contour of the base model on the front-end surface perpendicular to the direction of the air flow. When the train moves forward, large drag forces, distributed evenly on the front-end of the train surface were observed. The maximum static pressure on the base model was determined to be 2.87 *kPa* through numerical simulation. Near the edges, the pressure is minimum. More effort and fuel is required to overcome large drag forces due to this pressure on the train front end to move forward smoothly. This shows that there is a need to improve the design of the front-end of train base model to reduce pressure region which leads to drag.

The design of the front-end nose profile of the train can be expressed in terms of geometric parameters which include A-pillar roundness (R_1), nose length (l_1) which controls shrinking of nose, and bluntness of nose (l_2). By varying these geometrical parameters appropriately, different train node models were obtained on which CFD was conducted to analyze flow characteristics. The influence of these independent variables on the coefficient of drag was determined for aerodynamic performance improvement. Based on CFD analysis, Model 8 was found to have minimum drag coefficient, thus drag force on the train surface due to low pressure as shown in Figure 9b. Therefore, this model was chosen as the best / optimum model under specified operating conditions that can be used for efficient and better train performance.

The pressure contour on the front-end of the optimum train model shows the maximum static pressure equal to 2.76 *kPa*. The region of the pressure was converged at the train nose. However, the rest of the train surface has minimum pressure values. In comparison to base model, the optimum model has the characteristics to reduce the pressure gradient and adverse pressure effects on the front-end leading to a better design as per requirement.

The streamlines of the air flow are tangent to the instantaneous velocity as shown in Figure 10. These streamlines are helpful in visualizing the flow over train. A small marked element of the fluid on the streamline path can be used to determine the flow characteristics. Figure 10 provides comparison of effectiveness of optimum model over base model through streamlines. The streamlines around base model appears to be closer and overlapping to each other. Air velocity at train surface is zero due to no slip condition. However, streamlines away from surface exhibit increasing velocity due to boundary layer thickness.

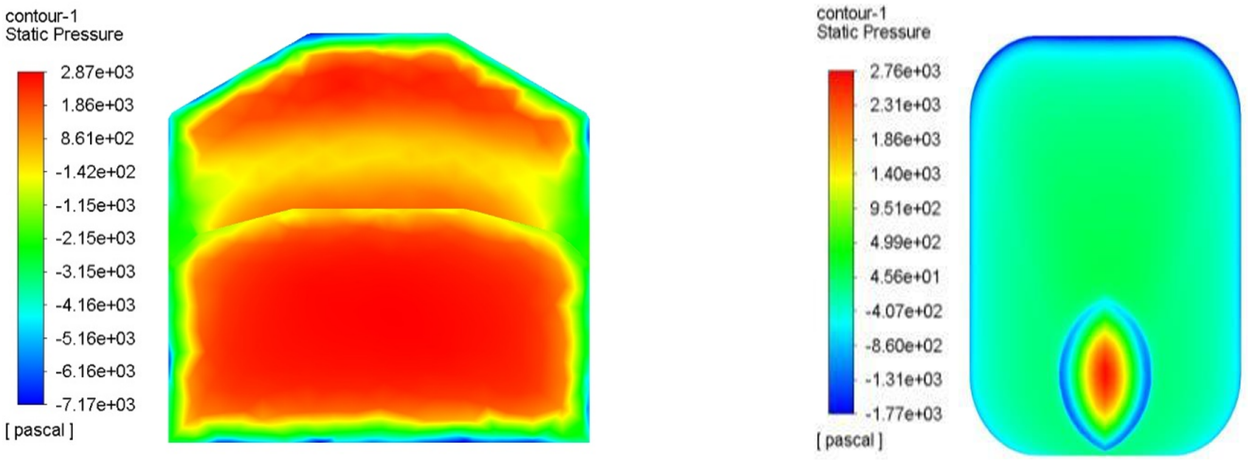

(a) Base model pressure contour (b) Optimum model pressure contour (Model 8)

FIGURE 9. Comparison of pressure contours on front surface of base and optimum Models

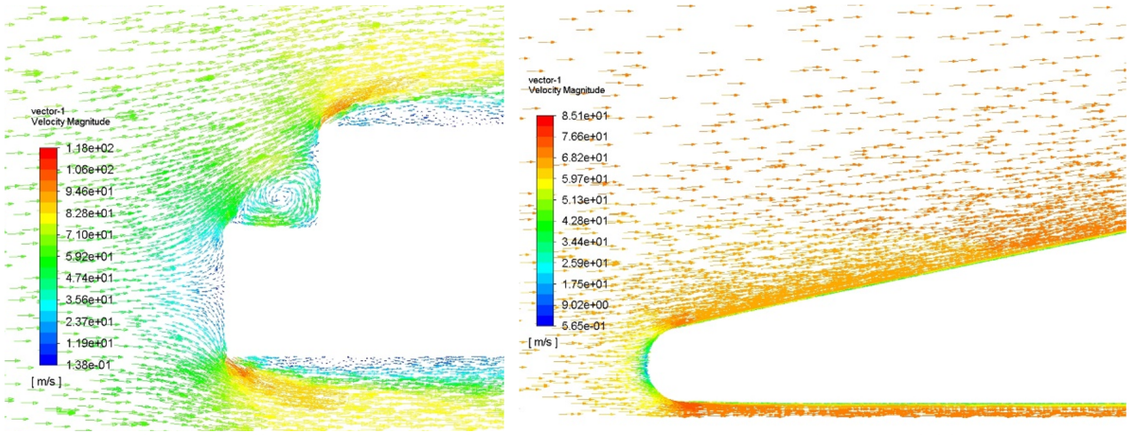

(a) Flow streamlines over base model (b) Flow over optimum model in vector form

FIGURE 10. Coarse flow pattern over train models

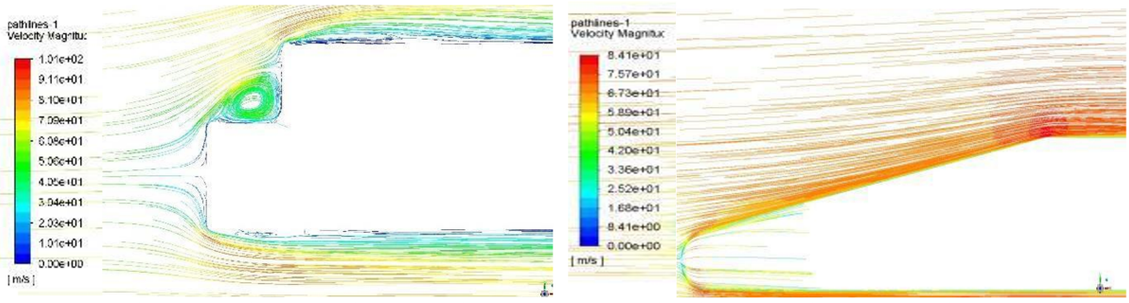

(a) Flow streamlines over base model (b) Flow streamlines over optimum model

FIGURE 11. Refined flow pattern over train models

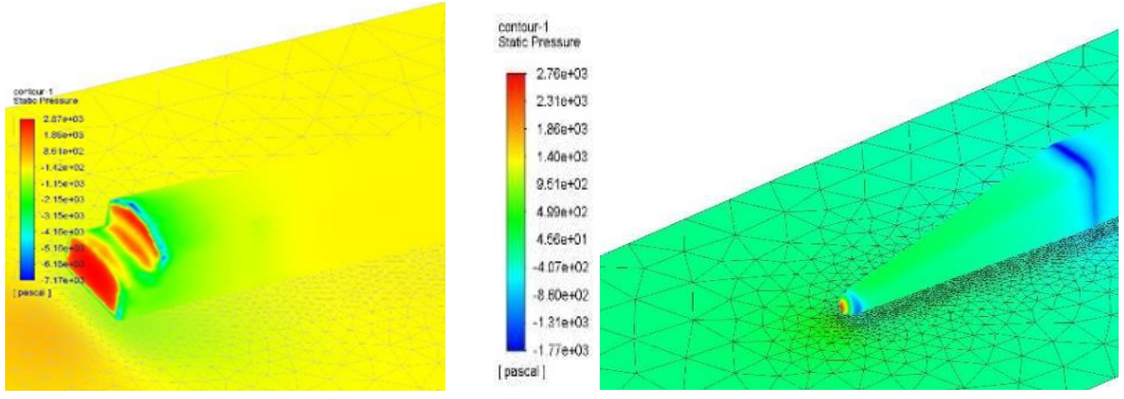

(a) Pressure contour over surface and surrounding of base model (b) Pressure contour over surface and surrounding of optimum model

FIGURE 12. Pressure contour plots over the surface and surroundings of train models

The front end of the base model is under a mixed flow condition creating a vortex. Near the sharp edges of the train, a sudden increase in the velocity was observed. Its magnitude is larger as compared to fluid particles in other regions. In all of the improved models with curved nose profile, the flow separation and vortex creation at the front surface were reduced. The air flow over optimum model became more streamlined as shown in Figure 10b. Due to the efficient design of the front-end of train, the vortex creation and adverse pressure region were greatly reduced.

A more refined flow of the streamlines and vector flow is presented in Figure 11. Around the base model, the vortex creation becomes more visible and zero-velocity due to no slip condition becomes prominent. The surface perpendicular to the air flow direction causes these streamlines to change their direction abruptly which results in the drag as shown in Figure 11a. This causes the utilization of more fuel and effort to overcome frictional / retarding forces. In Figure 11b, flow streamlines over optimum model shows significant reduction of vortex, high pressure regions and minimum velocity in nose profile. The streamlines were not overlapping and remained smooth, which is in accordance with the findings of Meng et al. (2021), Ding et al. (2016), Paniagua et al. (2019). Maximum velocity near the top end of the train surface was observed due to minimum boundary layer thickness, thus reducing drag.

The optimum train nose profile causes the flow to change its direction smoothly by exerting minimum drag thus making fuel consumption more efficient. Therefore, the optimum model provides a better flow characteristic in terms of drag, boundary layer and velocity and pressure distributions.

The pressure distribution along the fixed surface and the surrounding for the base and the optimum train models is presented in Figure 12. In case of base model, the distribution of pressure is larger at the front face as shown in Figure 12a. The reason can be attributed to the steep surface near the front face, larger pressure region and turbulent flow conditions. The static pressure contour of the optimum model in Figure 12b shows reduced pressure distribution near the front end of train nose with maximum value equal to 2.76 *kPa*. The surfaces around the train is subjected to medium pressure whose magnitude is nearly uniform and equal to the surrounding fluid domain. The optimum train design may be complex in comparison to the base model. However, the design effort for optimum model might significantly improve aerodynamic characteristics while reducing drag which in turn lessens the fuel consumption.

CONCLUSIONS

High speed trains are continuously being innovated by design and through structural and material improvements. Train nose is one of the structural components having a significant impact on train's aerodynamic performance. In this study, investigation of the influence of various train nose profile geometric parameters on aerodynamic drag was carried out using Computational Fluid Dynamics. These geometric parameters include A-pillar roundness, nose bluntness and nose length which controls its shrinkage. The base model of a train design was considered for improvement by varying nose geometric parameters. Various train models were developed in Solid Works for evaluating aerodynamic performance in FLUENT. The aerodynamic performance in terms of pressure distribution, velocity profiles, pressure gradient, boundary layer, wake region, vortex formation, drag and lift were ascertained to identify better model. The significance of adverse pressure and drag reduction can be attributed to the improvement in fuel economy, safety, lower vibrations, reliability and higher performance. Less power is consumed to overcome the drag on the surface profile of the optimized model as compared to base model due to smooth airflow and streamlines. Following conclusions were drawn from the numerical computations regarding train aerodynamic performance:

1. The coefficient of drag hence the drag force has inverse relationship with A-pillar roundness linked with nose tip curvature.
2. The coefficient of drag decreases with the increase of nose bluntness.
3. The influence of nose length on drag is contrary to A-pillar roundness and nose bluntness. The increase in nose length, that controls shrinking of the nose, causes an increase in coefficient of drag.
4. The nose length that controls its shrinkage has been observed to be the more influential parameter as compared to other nose geometric parameters considered in this research, in terms of effect on aerodynamic drag.
5. The optimum model has been observed to have least adverse pressure gradient, wake region and drag along with highly smooth flow streamlines.

As speeds and capabilities of high-speed trains are set to keep on improving with the developing world moving towards this transport system, the scope and importance of this research field is at a high level. The developing world can establish design and structural changes to the trains for improved performance and fuel consumption. It is an interesting proposition to study the influence of other geometric parameters of train nose along with tunnel passages, platforms, crosswinds and trains passing each other, on aerodynamic characteristics.

ACKNOWLEDGEMENT

The authors would like to thank University of Lahore, Pakistan for their support.

DECLARATION OF COMPETING INTEREST

None

REFERENCES

Anderson, J.D. and Wendt, J. 1995. *Computational Fluid Dynamics* (Vol. 206, p. 332). New York: McGraw-Hill.

Bugvi, S. A., Hameed, K., Hussain, A., & Tabassum, S. A. (2021). The CPEC Supply Web Framework in Context of Modern Manufacturing. *Jurnal Kejuruteraan* 33(1): 39-46.

Chen, X.D., Liu, T.H., Zhou, X.S., Li, W.H., Xie, T.Z. and Chen, Z.W., 2017. Analysis of the aerodynamic effects of different nose lengths on two trains intersecting in a tunnel at 350 km/h. *Tunnelling and Underground Space Technology* 66: 77-90.

Chen, G., Li, X.B., Liu, Z., Zhou, D., Wang, Z., Liang, X.F. and Krajnovic, S. 2019. Dynamic analysis of the effect of nose length on train aerodynamic performance. Journal of Wind Engineering and Industrial Aerodynamics, 184, pp.198-208.

Chen, Z.W., Liu, T.H., Yan, C.G., Yu, M., Guo, Z.J. and Wang, T.T. 2019. Numerical simulation and comparison of the slipstreams of trains with different nose lengths under crosswind. *Journal of Wind Engineering and Industrial Aerodynamics* 190: 256-272.

Ding, S. S., Li, Q., Tian, A. Q., Du, J., & Liu, J. L. 2016. Aerodynamic design on high-speed trains. *Acta Mechanica Sinica* 32(2): 215-232.

Jin, X.S. 2018. Key problems faced in high-speed train operation. In China's High-Speed Rail Technology (pp. 27-45). Springer, Singapore.

Li, W. H., Liu, T. H., Zhang, J., Chen, Z. W., Chen, X. D., & Xie, T. Z. 2017. Aerodynamic study of two opposing moving trains in a tunnel based on different nose contours. *Journal of Applied Fluid Mechanics* 10(5): 1375-1386.

G., Zhou, D. and Chen, Z., 2019. Impact of different nose lengths on flow-field structure around a high-speed train. *Applied Sciences* 9(21): 4573.

Ku, Y.-C., Rho, J.-H., Yun, S.-H., Kwak, M.-H., Kim, K.-H., Kwon, H.-B., Lee, D.-H., 2010.

Optimal cross-sectional area distribution of a high-speed train nose to minimize the tunnel micro-pressure wave. *Struct. Multidiscip. Optim.* 42: 965–976

Li, W., Liu, T., Chen, Z., Guo, Z. and Huo, X., 2020. Comparative study on the unsteady slipstream induced by a single train and two trains passing each other in a tunnel. *Journal of Wind Engineering and Industrial Aerodynamics* 198: 104095.

Meng, S., Meng, S., Wu, F., Li, X. and Zhou, D., 2021. Comparative analysis of the slipstream of different nose lengths on two trains passing each other. *Journal of Wind Engineering and Industrial Aerodynamics* 208: 104457.

Mughal, K.H., Bugvi, S.A., Qureshi, M.A.M., Khan, M.A. and Hayat, K., 2021. Numerical Evaluation of Contemporary Excavator Bucket Designs using Finite Element Analysis. *Jurnal Kejuruteraan* 33(3): 579-591.

Mughal, K.H., Qureshi, M.A.M. and Raza, S.F., 2021. Novel ultrasonic horn design for machining advanced brittle composites: A step forward towards green and sustainable manufacturing. *Environmental Technology & Innovation* 23: 101652.

Mughal, K.H., Qureshi, M. A. M., Qaiser, A. A., Khalid, F. A., Maqbool, A., Raza, S. F., Ahmad, S. and Zhang, J. 2022. Numerical Investigation of the Effect of Uniform Cutout on Performance of Ultrasonic Horn for Machining Nomex Honeycomb Core Material. *Jurnal Kejuruteraan 34(3).*

Munoz-Paniagua, J., García, J., Crespo, A., 2014. Genetically aerodynamic optimization of the nose shape of a high-speed train entering a tunnel. *Journal of Wind Engineering and Industrial Aerodynamics* 130: 48-61.

Munoz-Paniagua, J., García, J., 2020. Aerodynamic drag optimization of a high-speed train. *Journal of Wind Engineering and Industrial Aerodynamics* 204: 104215.

Muñoz-Paniagua, J. and García, J., 2019. Aerodynamic surrogate-based optimization of the nose shape of a high-speed train for crosswind and passing-by scenarios. *Journal of Wind Engineering and Industrial Aerodynamics*,184: 139-152.

Miyachi, T., Kikuchi, K. and Tebbutt, J.A., 2020. Modeling pressure variations generated by short train passing in open air. *Journal of Sound and Vibration* 485: 115543.

Munoz, P.J., Garcia, J., Crespo, A. and Laspougeas, F., 2015. Aerodynamic optimization of the nose shape of a train using the adjoint method.

Niu, J., Wang, Y., Zhang, L. and Yuan, Y., 2018. Numerical analysis of aerodynamic characteristics of high-speed train with different train nose lengths. *International Journal of Heat and Mass Transfer* 127:188-199.

Niu, J.Q., Zhou, D., Liang, X.F., Liu, S. and Liu, T.H., 2018. Numerical simulation of the Reynolds number effect on the aerodynamic pressure in tunnels. *Journal of Wind Engineering and Industrial Aerodynamics* 173: 187-198.

Niu, J., Zhou, D., Liang, X., Liu, T. and Liu, S., 2017. Numerical study on the aerodynamic pressure of a metro train running between two adjacent platforms. *Tunnelling and Underground Space Technology* 65: 187-199.

Niu, J., Wang, Y. and Liu, F., 2020. Numerical study on the effect of damaged windows on aerodynamic characteristics of passenger trains under strong crosswind. Proceedings of the Institution of Mechanical Engineers, Part C: *Journal of Mechanical Engineering Science* 234(15): 2994-3003.

Raghunathan, R.S., Kim, H.D. and Setoguchi, T., 2002. Aerodynamics of high-speed railway train. *Progress in Aerospace Sciences* 38(6-7): 469-514.

Shuanbao, Y., Dilong, G., Zhenxu, S., Guowei, Y. and Dawei, C., 2014. Optimization design for aerodynamic elements of high-speed trains. *Computers & Fluids* 95: 56-73.

Viviani, A., Aprovitola, A., Pezzella, G. and Rainone, C., 2021. CFD design capabilities for next generation high-speed aircraft. *Acta Astronautica* 178: 143-158.

Zhou, L. & Shen, Z., 2011. Progress in high-speed train technology around the world. *Journal of Modern Transportation* 19(1): 1-6.

Zhou, L. and Shen, Z. 2011. Progress in high-speed train technology around the world. Journal of Modern Transportation 19(1): 1-6.

Zhang, J., Ding, G.F., Zhou, Y.S., Jiang, J., Ying, X. and Qin, S.F., 2014. Identification of key design parameters of high-speed train for optimal design. *The International Journal of Advanced Manufacturing Technology* 73(1): 251-265.

Zampieri, A., Rocchi, D., Schito, P. and Somaschini, C., 2020. Numerical-experimental analysis of the slipstream produced by a high speed train. *Journal of Wind Engineering and Industrial Aerodynamics* 196:104022.